ACS APPLIED MATERIALS & INTERFACES

# Sacrificial Poly(propylene carbonate) Membrane for Dispersing Nanoparticles and Preparing Artificial Solid Electrolyte Interphase on Li Metal Anode

Qipeng Yu, Weicong Mai, Weijiang Xue, Guiyin Xu, Qi Liu, Kun Zeng, Yuanming Liu, Feiyu Kang, Baohua Li,* and Ju Li*

**Cite This:** *ACS Appl. Mater. Interfaces* 2020, 12, 27087−27094

Read Online

ACCESS | Metrics & More | Article Recommendations | Supporting Information

**ABSTRACT:** Lithium-metal batteries have been regarded as next-generation high-energy-density candidates beyond lithium-ion batteries. However, the lithium-morphology instabilities accompanied by continuous side reactions with electrolytes inevitably leads to dissatisfactory performances and even safety issues, where the unstable interface between lithium-metal anode and electrolytes has been regarded as the root cause. Artificial solid electrolyte interphase engineering has attracted a lot of attention to stabilize lithium-metal anodes. Here, a novel method with universality is reported to produce the organic−inorganic artificial solid electrolyte interphase. Using poly(propylene carbonate) as a sacrificial matrix, nanoparticles are dispersed on lithium-metal anodes surface uniformly to prepare artificial solid electrolyte interphase, where poly(propylene carbonate) turns into liquid propylene carbonate upon contact with lithium-metal anode. Silicon, $Li_{1.5}Al_{0.5}Ge_{1.5}(PO_4)_3$, or $Li_{1.4}Al_{0.4}Ti_{1.6}(PO_4)_3$ nanoparticles are coated to suppress lithium-morphology instabilities and demonstrated ~4 times longer cycle life. Preparing various organic/inorganic artificial solid electrolyte interphase is feasible by introducing various components in the fabrication process of poly(propylene carbonate) membrane, endowing this approach with huge potential in the research of artificial solid electrolyte interphase.

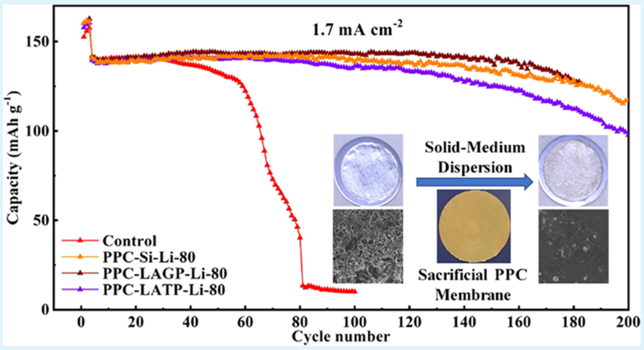

**KEYWORDS:** *lithium-metal anode, poly(propylene carbonate), solid electrolyte interphase, solid-medium approach, nanoparticles*

## INTRODUCTION

Lithium-metal anode (LMA) enables significantly higher energy densities than graphite-based lithium-ion batteries (LIBs).[1−6] However, lithium-morphology instabilities (LMI) negatively impact the cycle life and safety of the battery.[7−14] The naturally formed solid electrolyte interphases (NSEIs) in classic carbonate electrolytes are too thin and fragile to suppress LMI on their own.[15] To suppress LMI, electronically insulating, strong, and tough SEIs or separators are helpful, which allow $Li^+$ to cross but not electrons.[15−18] Recently, significant efforts have been made to modify SEI or create artificial SEI (ASEI),[19−44] like organic ASEI with enhanced mechanical strength,[20] Li-ion-affinity functional groups,[21] or single-ion conductivity,[22,23] or inorganic ASEI such as LiF,[24,25] or some lithiophilic or Li-alloy materials,[26,27] on LMAs *via* the vacuum deposition,[28−30] electrolyte adjustment,[24,31,33] liquid-medium coating,[20,21,23,34−43] *etc.*

Liquid-medium coating (*e.g.*, by spin coating) is often used to fabricate uniform thin films, where typically the desired ASEI components are dissolved or dispersed in a liquid solvent.[20,21,23,34−43] However, ASEI should be insoluble in liquid electrolytes of actual batteries for maintaining its stability on LMA. Thus, the selected liquid medium for dispersing generally has a stronger solubility than that of a typical electrolyte, such as dimethyl formamide (DMF), which inevitably had a bad effect on the highly reactive LMA.[35] For the sake of avoiding this bad effect, many studies only fabricated ASEI on Cu foils and need further electrochemical deposition of lithium, which is cumbersome.[37−43,45] In this paper, we outline a universal solid-medium dispersal approach. A solid membrane is prefabricated, which contains all of the necessary ASEI parts encased in a solid matrix. This prefabricated membrane is then simply mechanically pressed on top of the lithium-metal foil. The solid matrix turns into

**Received:** March 4, 2020
**Accepted:** May 20, 2020
**Published:** May 20, 2020

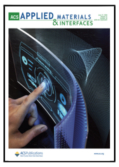

https://dx.doi.org/10.1021/acsami.0c04205
ACS Appl. Mater. Interfaces 2020, 12, 27087−27094

liquid upon contact with LMA, which helps to disperse the ASEI uniformly on the LMA.

Poly(propylene carbonate) (PPC) is used as biodegradable plastic, a sacrificial binder in ceramics sintering, and also as a solid electrolyte.[46,47] When PPC contacts lithium metal, it depolymerizes into propylene carbonate (PC), which is a common solvent of electrolytes in LIBs, and micromolecular segments.[48] It was reported that the depolymerization was mainly caused by the LiOH on the lithium metal, resembling the reaction of ester hydrolysis.[48] Based on these interesting properties, for the first time, PPC membranes containing desired nanoparticles (NPs), *e.g.*, silicon (Si), $Li_{1.5}Al_{0.5}Ge_{1.5}(PO_4)_3$ (LAGP), $Li_{1.4}Al_{0.4}Ti_{1.6}(PO_4)_3$ (LATP), *etc.*, are fabricated and put on LMA to form *in situ* ASEI films. With the presence of a liquid electrolyte, the NPs are simultaneously electrochemically shorted and form an *in situ* nanocomposite of NSEI with electrochemically lithiated NPs. The final nanocomposite film is thin, uniform, electronically insulating, strong, and tough and can function as an excellent ASEI.

The prefabrication of the PPC−solid membrane was typically done by facile solution casting. Si NPs were introduced into the PPC framework to form a free-standing membrane (PPC−Si) (Figure 1a,i). After contacting with LMA with a period of heating, the majority of PPC was depolymerized into PC and Si NPs were uniformly dispersed on the LMA (Figure 1b). With the appearance of liquid electrolyte and heat, Si would be lithiated electrochemically into $Li_xSi$ alloy, which was lithiophilic and can be regarded as a single-ion conductor and nucleation site to promote the uniform deposition of $Li_{BCC}$ metal in body-centered-cubic structure (Figure 1c).[29] Moreover, micromolecular segments of PPC can act as a binder and Li-ion-affinity component to form an organic−inorganic ASEI to suppress dendritic growth and improve the performance of LMAs (Figure 1d).[21] In addition, the main decomposition product PC could be easily removed by wiping and has good compatibility with LMAs. This sacrificial PPC-matrix can be easily applied to fabricate various organic−inorganic ASEI layers by introducing designed components into the free-standing membrane.

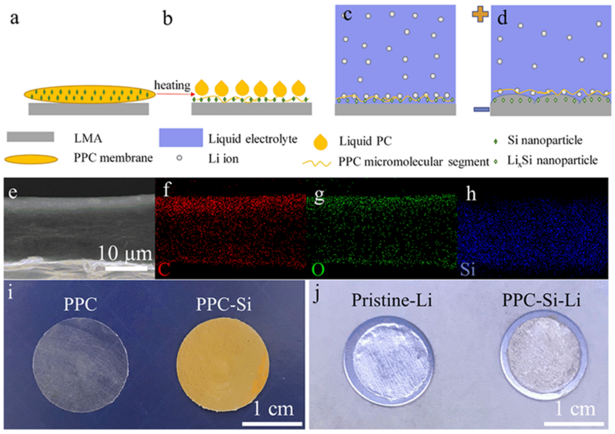

**Figure 1.** Schematic illustration of the function principle of the sacrificial PPC membrane for the fabrication of ASEI. Schematic illustration of (a) PPC−Si contacts with Li, (b) after heating, (c) after adding liquid electrolyte, and (d) uniform deposition of PPC−Si−Li. (e) Scanning electron microscopy (SEM) image of PPC−Si. Energy-dispersive X-ray spectra (EDS) mapping of (f) carbon, (g) oxygen, and (h) silicon elements of PPC−Si. Digital images of (i) PPC and PPC−Si membrane and (j) pristine Li and PPC−Si−Li.

## EXPERIMENTAL SECTION

**Materials.** Silicon nanoparticle with 30−50 nm grain size was purchased from Hongwu Nanometer Ltd. $Li_{1.5}Al_{0.5}Ge_{1.5}(PO_4)_3$ (LAGP) and $Li_{1.4}Al_{0.4}Ti_{1.6}(PO_4)_3$ (LATP) were obtained from Hefei Kejing Materials Technology Company. Poly(propylene carbonate) (PPC) was purchased from Sigma-Aldrich Corporation. Acetonitrile (AN) was purchased from Aladdin Industrial Corporation. $LiNi_{0.5}Co_{0.2}Mn_{0.3}O_2$ (NCM) and carbon-coated $LiFePO_4$ (LFP) were obtained from Canrd Corporation and dried in a vacuum oven at 80 °C for 12 h before use. Liquid electrolyte with the component of 1 M $LiPF_6$ in ethylene carbonate (EC)/diethyl carbonate (DEC) = 1/1, v/v was obtained from Canrd Corporation.

**Preparation of PPC Composite Membranes.** In typical processes, 0.15 g of PPC was mixed with 10 mL of AN and stirred under room temperature for 1 h to obtain a clear solution. Then, 3 mg of Si nanoparticle was dispersed in the above solution using an ultrasonic cell crusher. Afterward, the solution was spread on a poly(tetrafluoroethylene) plate (70 mm diameter) and heated at 60 °C for 12 h to evaporate AN, giving PPC−Si membranes. Si nanoparticle was replaced by LAGP or LATP powder to prepare PPC−LAGP or PPC−LATP membranes. Typically, the thickness of the PPC membranes was about 15 $\mu$m.

**Preparation of Artificial Solid Electrolyte Interphase (ASEI) on Lithium-Metal Anodes (LMAs) *via* Sacrificial PPC Membrane.** The PPC (composite) membranes were sandwiched with two lithium foils and fabricated into CR2032 coin-type cells in an argon-filled glovebox ($H_2O$, $O_2$ <0.1 ppm). The assembled cells were placed in an oven at 80 °C for 24 h and then disassembled in the argon-filled glovebox. Since PPC was mostly degraded into PC, the liquid on the surface of lithium foils was wiped by dust-free tissues to obtain the LMAs with ASEI for further characterization.

**Characterization.** X-ray diffraction (XRD) was performed using a Bruker D8 Advance diffractometer in an angle range of 10−80° ($2\theta$) using Cu K$\alpha$ radiation ($\lambda$ = 1.5418 Å). The characteristic chemical bonds of the samples were confirmed using a Fourier-transform infrared (FT-IR) spectrometer (Bruker Vertex70 instrument). The morphologies of the materials were investigated by using a field emission scanning electron microscope (SEM, Hitachi S4800) coupled with energy-dispersive X-ray spectra (EDS). The X-ray photoelectron spectra (XPS) of the samples were performed on a PHI 5000 VersaProbe II spectrometer using a monochromatic Al K$\alpha$ X-ray source calibrated with respect to carbon (284.8 eV). LMAs were transferred from the glovebox to the SEM and XPS instruments in a hermetically sealed container filled with the Ar gas to avoid contact with air.

**Electrochemical Measurements.** Electrochemical impedance spectroscopy (EIS) was measured by AC impedance spectroscopy using a VMP3 multichannel electrochemical station (Biologic Science Instruments) in the frequency range from 100 KHz to 0.01 Hz in certain time intervals after cell assembly. The symmetric cells were charged and discharged at a constant current of 0.5 or 1 mA $cm^{-2}$ with an areal capacity of 1 mAh $cm^{-2}$. For testing the batteries, the LFP or NCM electrodes were used as cathodes and prepared *via* mixing 90 wt % active material with 5 wt % super P and 5 wt % poly(vinylidene fluoride) (PVDF) on an Al foil with the loading mass of the active material of about 10 mg $cm^{-2}$. The prepared cathodes were dried at 120 °C under vacuum overnight and cut into 12 mm diameter disks for use. Celgard 2500 type polypropylene separators were placed between cathodes and anodes with a controlled amount of liquid electrolyte to fabricate CR2032 coin-type cells in an argon-filled glovebox. For LFP batteries, 60 $\mu$L of liquid electrolyte was added and ~500 $\mu$m thick Li foils were used. The cutoff voltages were set from 2.4 to 4.2 V and 1C current density was set as 170 mA $g^{-1}$. For NCM batteries, limited Li foils (~60 $\mu$m in thickness) and liquid electrolyte (20 $\mu$L) were applied to test the batteries in a more realized condition. The NCM cells were charged and discharged at

1C (150 mA $g^{-1}$) with a constant-voltage charge at 4.3 V before the current density reached 0.1C. For PPC−Si−Li−H, PPC−LAGP−Li−H, and PPC−LATP−Li−H anodes, the assembled batteries were placed in the oven at 80 °C for 24 h to make the reaction between Si, LAGP, LATP, and Li completely before cycling the batteries. Otherwise, the NPs may consume active lithium and worsen the performance of batteries. The charge and discharge measurements were carried out on a Land battery testing system at 25 °C.

## ■ RESULTS AND DISCUSSION

X-ray diffraction (XRD) and scanning electron microscopy (SEM) (Figures S1 and S2) confirmed that Si NPs with a primary particle size of less than 100 nm were crystalline without impurities.[49] The SEM and corresponding energy-dispersive X-ray spectra (EDS) mapping of PPC−Si indicated that the thickness of the PPC−Si membrane was ∼15 μm and Si NPs were uniformly dispersed inside the membrane (Figure 1e−h). The pure PPC membrane was transparent (Figure 1i). After introducing Si NPs into PPC−Si, it turned into tawny, which was consistent with the color of Si powder. The uniform coloration further indicated the homogeneous dispersion of Si (Figure 1i). The pristine Li foil had a shining metallic luster. After pressing and reacting with PPC−Si at 80 °C for 24 h and removing the generated liquid by wiping, the surface of Li (named PPC−Si−Li) changed into a little tawny with reduced gloss (Figure 1j), suggesting the Li foil was covered by Si NPs. The generated liquid was collected and characterized by FT-IR, with the results proving that PPC was depolymerized into PC after contacting with lithium metal (Figures S3 and S4).

The surface of pristine Li metal was relatively flat and smooth (Figure 2a). The surface of the reacted Li foil with pure PPC membrane (named PPC−Li) became slightly rougher, indicating that the micromolecular segments of PPC were left on LMAs (Figure 2b).[48] For PPC−Si−Li, Si NPs were uniformly dispersed on the surface of Li metal (Figure 2c). When the liquid electrolyte was added to PPC−Si−Li, Si NPs were electrochemically lithiated by $Li_{BCC}$ to form the $Li_xSi$ alloy.[29] To make this process spatially uniform and thorough before cycling of batteries, PPC−Si−Li with the liquid electrolyte was heated at 80 °C for 24 h (named PPC−Si−Li−H). Otherwise, the NPs may consume active lithium and worsen the performance of batteries. The morphology of PPC−Si−Li−H became compact as a result of the Li−Si alloy formation and the reaction of liquid electrolyte to form NSEI (Figure 2d). The cross-sectional SEM images of PPC−Si−Li−H further confirmed that a compact layer with a thickness of only ∼3 μm was covering only the top of Li metal (Figure S5). The EDS mapping of PPC−Si−Li demonstrated that the surface was uniformly covered by Si NPs (Figure 2e−h). It has been reported that dendrites could be suppressed when the modulus of the separator or electrolyte is improved. The Young's modulus of the ASEI on PPC−Si−Li−H was measured to be 12.26 GPa (Figure S6), which is significantly higher than that of the NSEI (∼0.7 GPa) and lithium metal (4.9 GPa).[50,51]

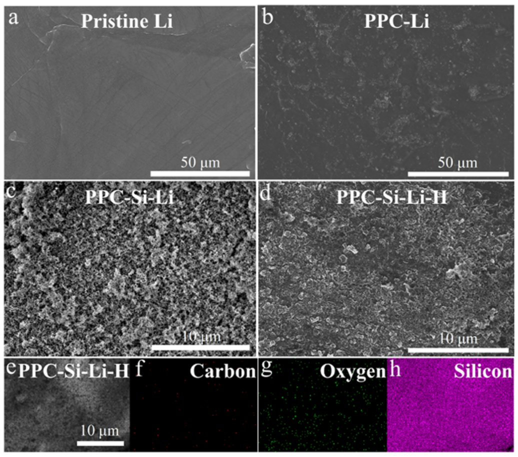

**Figure 2.** Surface morphology of lithium metal. SEM images of (a) pristine Li, (b) PPC−Li, (c) PPC−Si−Li, (d) PPC−Si−Li−H, and (e) PPC−Si−Li−H, and the corresponding EDS of (f) carbon, (g) oxygen, and (h) silicon element.

The C 1s spectrum in the X-ray photoelectron spectra (XPS) showed that the PPC treatment introduced more organic groups on the surface of LMAs to form organic ASEI as the intensity of the signal with higher binding energy increased (Figure 3b). The peaks at ∼286.5 and ∼288.5 eV represent the binding of C−O and O═C−O from the PPC segments.[48] For the Si 2p spectrum of pristine Si (Figure 3e), the first peak at ∼99.5 eV can be assigned to the bulk silicon and the other one was assigned to the surface silicon oxide (∼103 eV for Si−O).[52] After the dispersion of Si NPs on Li metal, a new peak at ∼98.5 eV can be attributed to the formation of the $Li_xSi$ alloy (Figure 3g).[53] For PPC−Si−Li−H, the weak signal of the Si 2p spectrum indicated that the NSEI layer covered the surface (Figure 3h), which was consistent with the SEM results (Figure 2d).[53]

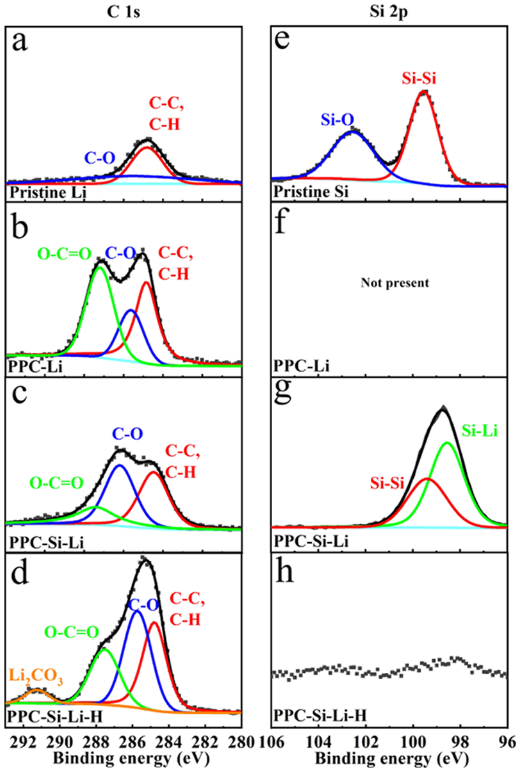

**Figure 3.** Surface chemistry revealed by XPS analysis. C 1s spectra of (a) pristine Li, (b) PPC−Li, (c) PPC−Si−Li, and (d) PPC−Si−Li−H. Si 2p spectra of (e) pristine Si, (f) PPC−Li, (g) PPC−Si−Li, and (h) PPC−Si−Li−H.

The surface morphologies of LMAs with different areal-deposition capacities are compared in Figures 4 and S7. All

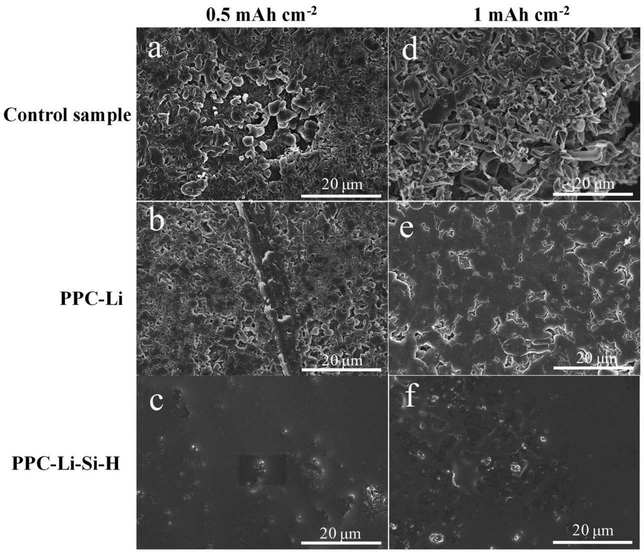

**Figure 4.** Surface morphology of LMA. SEM images of LMA at an areal-deposition capacity of 0.5 mAh $cm^{-2}$ of (a) control sample, (b) PPC−Li, and (c) PPC−Si−Li−H. SEM images of LMA at an areal-deposition capacity of 1 mAh $cm^{-2}$ of (d) control sample, (e) PPC−Li and (f) PPC−Si−Li−H.

experiments were conducted at a current density of 0.5 mA $cm^{-2}$. The LMAs without modification normally deposited into a mossy structure in the carbonate electrolytes (Figure 4a,d).[10,19,20,22,45] With the increased capacity to 2 and 3 mAh $cm^{-2}$, more and more whiskers and dendrite-like Li with high specific surface were formed, and more electrolyte was consumed to form the NSEI (Figure S7a,d).[19,41] For PPC−Li, the polar functional groups in the micromolecular segments of PPC might act as Li-ion-affinity functional groups to self-concentrate Li ions.[21] Therefore, it can mitigate the concentration polarization near the electrode surface to some extent and promote the formation of a compact surface (Figure 4b,e). It is worth noting that LiOH on the lithium metal, which is the main cause of depolymerization, was finite; PPC micromolecular segments would not entirely depolymerize into PC and could be maintained on the LMA.[48] The difference is even more pronounced in PPC−Si−Li−H (Figure 4c,f). A relatively smooth and compact structure was presented for the areal-deposition capacity of 0.5 and 1 mAh $cm^{-2}$ (Figure 4c,f). Moreover, Si NPs were embedded into the lithium metal, which could serve as nucleation sites and structural support for LMAs. After 100 cycles of 1 mAh $cm^{-2}$ deposition−stripping process, Si NPs were still dispersed uniformly on the surface of LMAs without detachment into the liquid electrolyte due to the bonding function of PPC (Figure S8). Such a compact structure *via* the uniform deposition can absolutely improve the electrochemical performance of LMAs with less consumption of the electrolyte and lithium metal.[20,26,45]

Symmetric lithium-metal cells were assembled and electrochemical impedance spectroscopy (EIS) were measured after different periods to further investigate the interfacial stability of different LMAs (Figure 5a). The total resistance of the control sample increased continuously over time, indicating that parasitic side reactions happened rampantly between the bare LMAs with liquid electrolyte.[15] After 24 h, it can be deduced that the stable interfaces were formed on PPC−Li because the resistance stopped to increase notably. The impedance spectroscopy of the control sample and PPC−Li showed a similar shape, which indicated that the interfacial properties were similar, while that of the PPC−Li−Si−H was characterized by two semicircles. The additional semicircle corresponds to the interfacial resistance introduced by Si NPs, which could be assigned to the ionic conductive property of $Li_xSi$.[54] It is worth noting that the total resistance of PPC−Si−Li−H was smaller than that of the control sample or PPC−Li at any stage, which implied that the introduction of such a compact and ionic conductive layer could restrain the side reaction and stabilize the interfaces. It could also be speculated that the conductivity of the ASEI on the PPC−Si−Li−H was

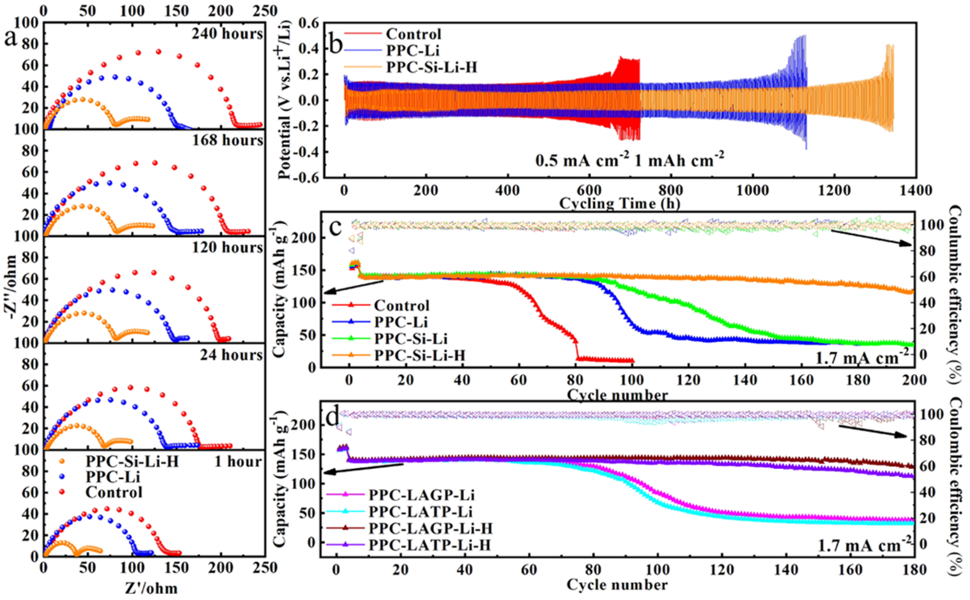

**Figure 5.** Electrochemical performance of different LMAs with or without ASEI. (a) EIS plots of the symmetric cells with different time intervals after cell assembly. (b) Lithium plating/stripping curves of symmetric cells at a current density of 0.5 mA $cm^{-2}$. (c) Cycling performance of LFP/Li cell with PPC−Si−Li and (d) PPC−solid electrolyte−Li at 1C.

higher than that of the ASEI on the PPC−Li and the NSEI on the pristine Li during the whole stages. The Bode impedance spectra of control sample, PPC−Li, and PPC−Si−Li−H are displayed in Figure S9, with the peaks at high frequency appearing for all samples while a unique peak at low frequency appearing for PPC−Si−Li−H, which could be regarded as additional electrochemical processes, corresponding to the Nyquist impedance spectra in Figure 5a. Such an improvement was further emphasized by investigating the interfacial resistance change of control sample and PPC−Li after heating at 80 °C for 24 h (named Control-H and PPC−Li−H, respectively). The continuously and significantly increased resistance of Control-H illustrated that heating aggravated side reaction between LMAs and electrolyte and a more unstable interphase was formed (Figure S10). In comparison, the resistance of PPC−Li−H gently increased, indicating the protective effect of the ASEI formed by pure PPC. According to the above results, PPC−Si−Li−H exhibited the lowest resistance and the most stable interphase, indicating it could remarkably resist the side reactions. The galvanostatic cycling test of symmetric cells further confirmed the above conclusions (Figures 5b and S11). PPC−Li showed improved stability compared with the control sample, while PPC−Si−Li−H exhibited the highest stability with over 1300 h of low polarization at 0.5 mA $cm^{-2}$. In comparison, the control sample only remained stable for 500 h at 0.5 mA $cm^{-2}$, indicating significant improvement by such an ASEI approach. Smaller polarization and smoother curves of PPC−Si−Li−H in the galvanostatic cycling test of symmetric cells at increased current densities (Figure S12) proved that such ASEI had improved charge-transfer kinetics. The exchange current densities ($I_0$) of PPC−Si−Li−H ($I_0$ = 0.334 mA $cm^{-2}$) is about twice that of the control sample ($I_0$ = 0.164 mA $cm^{-2}$), which was calculated from the Tafel plots, also indicating the faster charge-transfer kinetics in PPC−Si−Li−H (Figure S13). Such fast interfacial kinetics would benefit low polarization during Li electrodeposition.

$LiFePO_4$ (LFP) cathodes with active materials loading of ∼10 mg $cm^{-2}$ were applied to assemble asymmetric cell at a current density of 1.7 mA $cm^{-2}$ to further verify the effect of this strategy. Carbonate electrolyte without fluoroethylene carbonate (FEC) was used. The control samples only stably cycled for about 40 cycles (Figure 5c) and then the capacity dropped rapidly, which illustrated that the carbonate electrolyte was essentially unstable with LMAs.[15] Considering that excess electrolyte (60 $\mu$L) and anode (∼500 $\mu$m) were used, exhaustion of electrolyte or lithium inventory should not be the cause. LMI, as shown in Figure 4a,d in the control sample, led to more being NSEI formed and porous dead Li covering the LMAs, which should be the main reason for the increase in polarization and rapid drop of capacity (Figure S14a).[9] PPC−Si−Li without the heat treatment also exhibited an inferior performance because the Si NPs were not completely reduced at the initial stage (the ASEI is therefore not well-formed), which might cause electrolyte localization and localized corrosion of the metal foil anode.[16,55,56] After sufficient reactions between Si and Li, PPC−Si−Li−H delivered ∼4× longer cycle life than the control sample. The low polarization of PPC−Si−Li−H shown in Figure S14b during cycling is attributed to the suppression of LMI by our ASEI.[18] This effect could reduce the consumption of electrolyte and the formation of dead lithium, thus restraining the significant increase of resistance. The d$Q$/d$V$ plots also provided solid evidence of the improvement of stability and reversibility introduced by such ASEI (Figure S15).

Solid electrolytes LAGP and LATP NPs were also applied to demonstrate the wide applicability of this sacrificial PPC-matrix method (Figure 5d). LAGP and LATP with Na super ion conductor (NASICON) phase were reported to be intercalated by lithium at the potential under 0.5 V *vs* $Li^+$/Li or contact with lithium metal and formed a mixed (ionic/electronic) conducting structure.[54,57] Both LAGP and LATP bought conspicuous improvement in electrochemical performance, which was similar to that achieved by Si. That is, when heated at 80 °C for 24 h, significant improvement can be achieved, while only slight promotion was made without the heat treatment. LAGP and LATP were regarded as single-ion conductors, so $Li_xSi$ NPs could also serve as a single-ion conductor on the LMAs to mitigate the concentration polarization for the promotion of a uniform deposition. In addition, Figure S16 shows the chronoamperometry profile of lithium symmetric cells under a polarization voltage and the corresponding EISs before and after polarization. The lithium transference number ($t_+$) of PPC−Si−Li−H was calculated as 0.64, which is around twice that of the control sample (0.35). The significantly improved $t_+$ of PPC−Si−Li−H might be caused by $Li_xSi$ NPs, which could also act as a single-ion conductor on the LMAs. Batteries with more realistic parameters (leaner electrolyte of 20 $\mu$L, and $Li_{BCC}$ foil of 60 $\mu$m thickness) also showed that the ASEI had beneficial effects (Figure S17). In such rigorous conditions, the control sample could only be maintained stable for about 20 cycles with a sudden drop, which indicated that electrolyte and anode decreased and active Li exhausted faster. The Coulombic efficiency dropped significantly in the 20th cycle, demonstrating the generation of a large amount of irreversible Li. PPC−Si−Li−H exhibited more than two times longer life than the control sample, showing the effectiveness of such ASEI in promoting LMAs even in such harsh conditions.

## ■ CONCLUSIONS

In this work, a novel and facile solid-medium dispersal approach to fabricate organic−inorganic ASEI on LMA has been reported. This method was based on the depolymerization of PPC into liquid PC when in direct contact with Li metal. Si, LAGP, and LATP NPs were selected as examples to demonstrate the universality of this uniform dispersal method. With such ASEI, and prelithiated $Li_xSi$ NPs serving as nucleation sites, lithium metal cells delivered ∼4× longer cycling life than the control samples. This method can be applied to fabricate not only other inorganic ASEI but also various organic ASEI by simply blending the desired organic components in the prefabricated PPC membrane. The main depolymerization product PC has good compatibility with LMAs, while other solvents for fabricating ASEI might cause severe undesirable reactions.[35] Therefore, this universal method has a large potential for future ASEI development.

## ■ ASSOCIATED CONTENT

### Supporting Information

The Supporting Information is available free of charge at https://pubs.acs.org/doi/10.1021/acsami.0c04205.

XRD, SEM images of Si NPs, FT-IR of Si NPs and PPC membranes, SEM images of ASEI layer, SEM and EDS images of cycled Li foils, mechanical property of ASEI, EIS plots of the symmetric cells after heating, SEM images of LMA at higher deposition capacity, Bode impedance spectra, Tafel plots, lithium plating/stripping curves of symmetric cells, d$Q$/d$V$ plots, lithium transference number, charge−discharge curves in different cycles of batteries, and cycling performance of NCM/Li cell with less electrolyte and anode and the corresponding curves (PDF)

## AUTHOR INFORMATION

### Corresponding Authors

**Baohua Li** − *Shenzhen Key Laboratory on Power Battery Safety Research and Shenzhen Geim Graphene Center, Tsinghua Shenzhen International Graduate School, Shenzhen 518055, China*; orcid.org/0000-0001-5559-5767; Email: libh@mail.sz.tsinghua.edu.cn

**Ju Li** − *Department of Nuclear Science and Engineering and Department of Materials Science and Engineering, Massachusetts Institute of Technology, Cambridge, Massachusetts 02139, United States*; orcid.org/0000-0002-7841-8058; Email: liju@mit.edu

### Authors

**Qipeng Yu** − *Shenzhen Key Laboratory on Power Battery Safety Research and Shenzhen Geim Graphene Center, Tsinghua Shenzhen International Graduate School, Shenzhen 518055, China; School of Materials Science and Engineering, Tsinghua University, Beijing 100084, China*

**Weicong Mai** − *Shenzhen Key Laboratory on Power Battery Safety Research and Shenzhen Geim Graphene Center, Tsinghua Shenzhen International Graduate School, Shenzhen 518055, China*

**Weijiang Xue** − *Department of Nuclear Science and Engineering and Department of Materials Science and Engineering, Massachusetts Institute of Technology, Cambridge, Massachusetts 02139, United States*; orcid.org/0000-0002-3060-4580

**Guiyin Xu** − *Department of Nuclear Science and Engineering and Department of Materials Science and Engineering, Massachusetts Institute of Technology, Cambridge, Massachusetts 02139, United States*; orcid.org/0000-0002-5959-4814

**Qi Liu** − *Shenzhen Key Laboratory on Power Battery Safety Research and Shenzhen Geim Graphene Center, Tsinghua Shenzhen International Graduate School, Shenzhen 518055, China; School of Materials Science and Engineering, Tsinghua University, Beijing 100084, China*

**Kun Zeng** − *Shenzhen Key Laboratory on Power Battery Safety Research and Shenzhen Geim Graphene Center, Tsinghua Shenzhen International Graduate School, Shenzhen 518055, China*

**Yuanming Liu** − *Shenzhen Key Laboratory on Power Battery Safety Research and Shenzhen Geim Graphene Center, Tsinghua Shenzhen International Graduate School, Shenzhen 518055, China; School of Materials Science and Engineering, Tsinghua University, Beijing 100084, China*

**Feiyu Kang** − *Shenzhen Key Laboratory on Power Battery Safety Research and Shenzhen Geim Graphene Center, Tsinghua Shenzhen International Graduate School, Shenzhen 518055, China; School of Materials Science and Engineering, Tsinghua University, Beijing 100084, China*

Complete contact information is available at: https://pubs.acs.org/10.1021/acsami.0c04205

### Author Contributions

The manuscript was written through contributions of all authors. All authors have given approval to the final version of the manuscript.

### Funding

This work was supported by the National Nature Science Foundation of China (No. 51872157), the Shenzhen Key Laboratory on Power Battery Safety Research (No. ZDSYS201707271615073), the Shenzhen Technical Plan Project (Nos. JCYJ20170412170911187 and JCYJ20170817161753629), the Special Fund Project for Strategic Emerging Industry Development of Shenzhen (No. 20170428145209110), the Guangdong Technical Plan Project (No. 2017B090907005), and the Local Innovative and Research Teams Project of Guangdong Pearl River Talents Program (2017BT01N111).

### Notes

The authors declare no competing financial interest.

## ACKNOWLEDGMENTS

Q.Y. acknowledges the support from the Chinese Scholarship Council. The Tsinghua University Materials and Devices Testing Center (Tsinghua Shenzhen International Graduate School, SIGS) was also gratefully acknowledged. J.L. and W.X. acknowledge the support from Samsung Advanced Institute of Technology. Q.Y. appreciates the company and support from Jiajia Dai during the COVID-19 pandemic.

## REFERENCES

(1) Lochala, J.; Liu, D.; Wu, B.; Robinson, C.; Xiao, J. Research Progress toward the Practical Applications of Lithium-Sulfur Batteries. *ACS Appl. Mater. Interfaces* **2017**, *9*, 24407−24421.

(2) Pervez, S. A.; Cambaz, M. A.; Thangadurai, V.; Fichtner, M. Interface in Solid-State Lithium Battery: Challenges, Progress, and Outlook. *ACS Appl. Mater. Interfaces* **2019**, *11*, 22029−22050.

(3) Xue, W.; Shi, Z.; Suo, L.; Wang, C.; Wang, Z.; Wang, H.; So, K. P.; Maurano, A.; Yu, D.; Chen, Y.; Qie, L.; Zhu, Z.; Xu, G.; Kong, J.; Li, J. Intercalation-conversion hybrid cathodes enabling Li−S full-cell architectures with jointly superior gravimetric and volumetric energy densities. *Nat. Energy* **2019**, *4*, 374−382.

(4) Xu, G.; Kushima, A.; Yuan, J.; Dou, H.; Xue, W.; Zhang, X.; Yan, X.; Li, J. Ad hoc solid electrolyte on acidized carbon nanotube paper improves cycle life of lithium−sulfur batteries. *Energy Environ. Sci.* **2017**, *10*, 2544−2551.

(5) Choudhury, S.; Wan, C. T.-C.; Al Sadat, W. I.; Tu, Z.; Lau, S.; Zachman, M. J.; Kourkoutis, L. F.; Archer, L. A. Designer interphases for the lithium-oxygen electrochemical cell. *Sci. Adv.* **2017**, *3*, No. e1602809.

(6) Liu, M.; Qin, X.; He, Y.-B.; Li, B.; Kang, F. Recent innovative configurations in high-energy lithium−sulfur batteries. *J. Mater. Chem. A* **2017**, *5*, 5222−5234.

(7) Liu, J.; Bao, Z.; Cui, Y.; Dufek, E. J.; Goodenough, J. B.; Khalifah, P.; Li, Q.; Liaw, B. Y.; Liu, P.; Manthiram, A.; Meng, Y. S.; Subramanian, V. R.; Toney, M. F.; Viswanathan, V. V.; Whittingham, M. S.; Xiao, J.; Xu, W.; Yang, J.; Yang, X.-Q.; Zhang, J.-G. Pathways for practical high-energy long-cycling lithium metal batteries. *Nat. Energy* **2019**, *4*, 180−186.

(8) Kushima, A.; So, K. P.; Su, C.; Bai, P.; Kuriyama, N.; Maebashi, T.; Fujiwara, Y.; Bazant, M. Z.; Li, J. Liquid cell transmission electron microscopy observation of lithium metal growth and dissolution: Root growth, dead lithium and lithium flotsams. *Nano Energy* **2017**, *32*, 271−279.

(9) Xiao, J. How lithium dendrites form in liquid batteries. *Science* **2019**, *366*, 426−427.
(10) Li, S.; Jiang, M.; Xie, Y.; Xu, H.; Jia, J.; Li, J. Developing High-Performance Lithium Metal Anode in Liquid Electrolytes: Challenges and Progress. *Adv. Mater.* **2018**, *30*, No. 1706375.
(11) Liu, L.; Sun, C. Flexible Quasi-Solid-State Composite Electrolyte Membrane Derived from a Metal-Organic Framework for Lithium-Metal Batteries. *ChemElectroChem* **2020**, *7*, 707−715.
(12) Zhang, W.; Yi, Q.; Li, S.; Sun, C. An ion-conductive Li7La3Zr2O12-based composite membrane for dendrite-free lithium metal batteries. *J. Power Sources* **2020**, *450*, No. 227710.
(13) Sun, C.; Liu, J.; Gong, Y.; Wilkinson, D. P.; Zhang, J. Recent advances in all-solid-state rechargeable lithium batteries. *Nano Energy* **2017**, *33*, 363−386.
(14) Qiu, G.; Sun, C. A quasi-solid composite electrolyte with dual salts for dendrite-free lithium metal batteries. *New J. Chem.* **2020**, *44*, 1817−1824.
(15) Cheng, X. B.; Zhang, R.; Zhao, C. Z.; Wei, F.; Zhang, J. G.; Zhang, Q. A Review of Solid Electrolyte Interphases on Lithium Metal Anode. *Adv. Sci.* **2016**, *3*, No. 1500213.
(16) Jiang, M.; Yu, Y.; Fan, H.; Xu, H.; Zheng, Y.; Huang, Y.; Li, S.; Li, J. Full-Cell Cycling of a Self-Supporting Aluminum Foil Anode with a Phosphate Conversion Coating. *ACS Appl. Mater. Interfaces* **2019**, *11*, 15656−15661.
(17) Liu, K.; Bai, P.; Bazant, M. Z.; Wang, C.-A.; Li, J. A soft non-porous separator and its effectiveness in stabilizing Li metal anodes cycling at 10 mA cm−2 observed in situ in a capillary cell. *J. Mater. Chem. A* **2017**, *5*, 4300−4307.
(18) Tang, Z.; Li, S.; Li, Y.; Xu, H.; Yu, Y.; Huang, Y.; Li, J. Lithium Metal Electrode Protected by Stiff and Tough Self-Compacting Separator. *Nano Energy* **2020**, *69*, No. 104399.
(19) Kim, M. S.; Ryu, J.-H.; Deepika; Lim, Y. R.; Nah, I. W.; Lee, K.-R.; Archer, L. A.; Il Cho, W. Langmuir−Blodgett artificial solid-electrolyte interphases for practical lithium metal batteries. *Nat. Energy* **2018**, *3*, 889−898.
(20) Zheng, G.; Wang, C.; Pei, A.; Lopez, J.; Shi, F.; Chen, Z.; Sendek, A. D.; Lee, H.-W.; Lu, Z.; Schneider, H.; Safont-Sempere, M. M.; Chu, S.; Bao, Z.; Cui, Y. High-Performance Lithium Metal Negative Electrode with a Soft and Flowable Polymer Coating. *ACS Energy Lett.* **2016**, *1*, 1247−1255.
(21) Li, G.; Liu, Z.; Wang, D.; He, X.; Liu, S.; Gao, Y.; AlZahrani, A.; Kim, S. H.; Chen, L. Q.; Wang, D. Electrokinetic Phenomena Enhanced Lithium-Ion Transport in Leaky Film for Stable Lithium Metal Anodes. *Adv. Energy Mater.* **2019**, *9*, No. 1900704.
(22) Tu, Z.; Choudhury, S.; Zachman, M. J.; Wei, S.; Zhang, K.; Kourkoutis, L. F.; Archer, L. A. Designing Artificial Solid-Electrolyte Interphases for Single-Ion and High-Efficiency Transport in Batteries. *Joule* **2017**, *1*, 394−406.
(23) Deng, K.; Han, D.; Ren, S.; Wang, S.; Xiao, M.; Meng, Y. Single-ion conducting artificial solid electrolyte interphase layers for dendrite-free and highly stable lithium metal anodes. *J. Mater. Chem. A* **2019**, *7*, 13113−13119.
(24) Lu, Y.; Tu, Z.; Archer, L. A. Stable lithium electrodeposition in liquid and nanoporous solid electrolytes. *Nat. Mater.* **2014**, *13*, 961−969.
(25) Fan, L.; Zhuang, H. L.; Gao, L.; Lu, Y.; Archer, L. A. Regulating Li deposition at artificial solid electrolyte interphases. *J. Mater. Chem. A* **2017**, *5*, 3483−3492.
(26) Liu, H.; Cheng, X.-B.; Huang, J.-Q.; Kaskel, S.; Chou, S.; Park, H. S.; Zhang, Q. Alloy Anodes for Rechargeable Alkali-Metal Batteries: Progress and Challenge. *ACS Mater. Lett.* **2019**, *1*, 217−229.
(27) Liang, X.; Pang, Q.; Kochetkov, I. R.; Sempere, M. S.; Huang, H.; Sun, X.; Nazar, L. F. A facile surface chemistry route to a stabilized lithium metal anode. *Nat. Energy* **2017**, *2*, No. 17119.
(28) Zhao, Y.; Amirmaleki, M.; Sun, Q.; Zhao, C.; Codirenzi, A.; Goncharova, L. V.; Wang, C.; Adair, K.; Li, X.; Yang, X.; Zhao, F.; Li, R.; Filleter, T.; Cai, M.; Sun, X. Natural SEI-Inspired Dual-Protective Layers via Atomic/Molecular Layer Deposition for Long-Life Metallic Lithium Anode. *Matter* **2019**, *1*, 1215−1231.
(29) Tang, W.; Yin, X.; Kang, S.; Chen, Z.; Tian, B.; Teo, S. L.; Wang, X.; Chi, X.; Loh, K. P.; Lee, H. W.; Zheng, G. W. Lithium Silicide Surface Enrichment: A Solution to Lithium Metal Battery. *Adv. Mater.* **2018**, No. e1801745.
(30) Kozen, A. C.; Lin, C.-F.; Pearse, A. J.; Schroeder, M. A.; Han, X.; Hu, L.; Lee, S.-B.; Rubloff, G. W.; Noked, M. Next-generation lithium metal anode engineering via atomic layer deposition. *ACS Nano* **2015**, *9*, 5884−5892.
(31) Zhao, Q.; Tu, Z.; Wei, S.; Zhang, K.; Choudhury, S.; Liu, X.; Archer, L. A. Building Organic/Inorganic Hybrid Interphases for Fast Interfacial Transport in Rechargeable Metal Batteries. *Angew. Chem., Int. Ed.* **2018**, *57*, 992−996.
(32) Tu, Z.; Choudhury, S.; Zachman, M. J.; Wei, S.; Zhang, K.; Kourkoutis, L. F.; Archer, L. A. Fast ion transport at solid−solid interfaces in hybrid battery anodes. *Nat. Energy* **2018**, *3*, 310−316.
(33) Ding, F.; Xu, W.; Graff, G. L.; Zhang, J.; Sushko, M. L.; Chen, X.; Shao, Y.; Engelhard, M. H.; Nie, Z.; Xiao, J.; Liu, X.; Sushko, P. V.; Liu, J.; Zhang, J. G. Dendrite-free lithium deposition via self-healing electrostatic shield mechanism. *J. Am. Chem. Soc.* **2013**, *135*, 4450−4456.
(34) Liu, Y.; Lin, D.; Yuen, P. Y.; Liu, K.; Xie, J.; Dauskardt, R. H.; Cui, Y. An Artificial Solid Electrolyte Interphase with High Li-Ion Conductivity, Mechanical Strength, and Flexibility for Stable Lithium Metal Anodes. *Adv. Mater.* **2017**, *29*, No. 1605531.
(35) Gao, Y.; Zhao, Y.; Li, Y. C.; Huang, Q.; Mallouk, T. E.; Wang, D. Interfacial Chemistry Regulation via a Skin-Grafting Strategy Enables High-Performance Lithium-Metal Batteries. *J. Am. Chem. Soc.* **2017**, *139*, 15288−15291.
(36) Gao, Y.; Yan, Z.; Gray, J. L.; He, X.; Wang, D.; Chen, T.; Huang, Q.; Li, Y. C.; Wang, H.; Kim, S. H.; Mallouk, T. E.; Wang, D. Polymer-inorganic solid-electrolyte interphase for stable lithium metal batteries under lean electrolyte conditions. *Nat. Mater.* **2019**, *18*, 384−389.
(37) Zhu, B.; Jin, Y.; Hu, X.; Zheng, Q.; Zhang, S.; Wang, Q.; Zhu, J. Poly(dimethylsiloxane) Thin Film as a Stable Interfacial Layer for High-Performance Lithium-Metal Battery Anodes. *Adv. Mater.* **2017**, *29*, No. 1603755.
(38) Luo, J.; Fang, C.-C.; Wu, N.-L. High Polarity Poly(vinylidene difluoride) Thin Coating for Dendrite-Free and High-Performance Lithium Metal Anodes. *Adv. Energy Mater.* **2018**, *8*, No. 1701482.
(39) Li, N.; Ye, Q.; Zhang, K.; Yan, H.; Shen, C.; Wei, B.; Xie, K. Normalized Lithium Growth from the Nucleation Stage for Dendrite-Free Lithium Metal Anodes. *Angew. Chem., Int. Ed.* **2019**, *58*, 18246−18251.
(40) Fan, W.; Zhang, R.; Wang, Z.; Lei, X.; Qin, C.; Liu, X. Facile fabrication of polyether sulfone (PES) protecting layer on Cu foil for stable Li metal anode. *Electrochim. Acta* **2018**, *260*, 407−412.
(41) Guo, Y.; Ouyang, Y.; Li, D.; Wei, Y.; Zhai, T.; Li, H. PMMA-assisted Li deposition towards 3D continuous dendrite-free lithium anode. *Energy Storage Mater.* **2019**, *16*, 203−211.
(42) Xu, B.; Zhai, H.; Liao, X.; Qie, B.; Mandal, J.; Gong, T.; Tan, L.; Yang, X.; Sun, K.; Cheng, Q.; Chen, M.; Miao, Y.; Wei, M.; Zhu, B.; Fu, Y.; Li, A.; Chen, X.; Min, W.; Nan, C.-W.; Lin, Y.-H.; Yang, Y. Porous insulating matrix for lithium metal anode with long cycling stability and high power. *Energy Storage Mater.* **2019**, *17*, 31−37.
(43) Zhao, Y.; Wang, D.; Gao, Y.; Chen, T.; Huang, Q.; Wang, D. Stable Li metal anode by a polyvinyl alcohol protection layer via modifying solid-electrolyte interphase layer. *Nano Energy* **2019**, *64*, No. 103893.
(44) Jin, Y.; Li, S.; Kushima, A.; Zheng, X.; Sun, Y.; Xie, J.; Sun, J.; Xue, W.; Zhou, G.; Wu, J.; Shi, F.; Zhang, R.; Zhu, Z.; So, K.; Cui, Y.; Li, J. Self-healing SEI enables full-cell cycling of a silicon-majority anode with a coulombic efficiency exceeding 99.9%. *Energy Environ. Sci.* **2017**, *10*, 580−592.
(45) Li, G.; Liu, Z.; Huang, Q.; Gao, Y.; Regula, M.; Wang, D.; Chen, L.-Q.; Wang, D. Stable metal battery anodes enabled by

polyethylenimine sponge hosts by way of electrokinetic effects. *Nat. Energy* **2018**, *3*, 1076−1083.

(46) Zhang, J.; Zhao, J.; Yue, L.; Wang, Q.; Chai, J.; Liu, Z.; Zhou, X.; Li, H.; Guo, Y.; Cui, G.; Chen, L. Safety-Reinforced Poly-(Propylene Carbonate)-Based All-Solid-State Polymer Electrolyte for Ambient-Temperature Solid Polymer Lithium Batteries. *Adv. Energy Mater.* **2015**, *5*, No. 1501082.

(47) Zhang, J.; Zang, X.; Wen, H.; Dong, T.; Chai, J.; Li, Y.; Chen, B.; Zhao, J.; Dong, S.; Ma, J.; Yue, L.; Liu, Z.; Guo, X.; Cui, G.; Chen, L. High-voltage and free-standing poly(propylene carbonate)/Li6.75La3Zr1.75Ta0.25O12 composite solid electrolyte for wide temperature range and flexible solid lithium ion battery. *J. Mater. Chem. A* **2017**, *5*, 4940−4948.

(48) Wang, C.; Zhang, H.; Li, J.; Chai, J.; Dong, S.; Cui, G. The interfacial evolution between polycarbonate-based polymer electrolyte and Li-metal anode. *J. Power Sources* **2018**, *397*, 157−161.

(49) Tian, H.; Tan, X.; Xin, F.; Wang, C.; Han, W. Micro-sized nano-porous Si/C anodes for lithium ion batteries. *Nano Energy* **2015**, *11*, 490−499.

(50) Zhang, X.; Wang, A.; Liu, X.; Luo, J. Dendrites in Lithium Metal Anodes: Suppression, Regulation, and Elimination. *Acc. Chem. Res.* **2019**, *52*, 3223−3232.

(51) Liu, Q.; Cai, B.; Li, S.; Yu, Q.; Lv, F.; Kang, F.; Wang, Q.; Li, B. Long-cycling and safe lithium metal batteries enabled by the synergetic strategy of ex situ anodic pretreatment and an in-built gel polymer electrolyte. *J. Mater. Chem. A* **2020**, *8*, 7197−7204.

(52) Radvanyi, E.; De Vito, E.; Porcher, W.; Jouanneau Si Larbi, S. An XPS/AES comparative study of the surface behaviour of nano-silicon anodes for Li-ion batteries. *J. Anal. At. Spectrom.* **2014**, *29*, 1120−1131.

(53) Chan, C. K.; Ruffo, R.; Hong, S. S.; Cui, Y. Surface chemistry and morphology of the solid electrolyte interphase on silicon nanowire lithium-ion battery anodes. *J. Power Sources* **2009**, *189*, 1132−1140.

(54) Yu, Q.; Han, D.; Lu, Q.; He, Y. B.; Li, S.; Liu, Q.; Han, C.; Kang, F.; Li, B. Constructing Effective Interfaces for Li1.5Al0.5Ge1.5-(PO4)3 Pellets To Achieve Room-Temperature Hybrid Solid-State Lithium Metal Batteries. *ACS Appl. Mater. Interfaces* **2019**, *11*, 9911−9918.

(55) Yu, Y.; Li, S.; Fan, H.; Xu, H.; Jiang, M.; Huang, Y.; Li, J. Optimal annealing of Al foil anode for prelithiation and full-cell cycling in Li-ion battery: The role of grain boundaries in lithiation/delithiation ductility. *Nano Energy* **2020**, *67*, No. 104274.

(56) Fan, H.; Chen, B.; Li, S.; Yu, Y.; Xu, H.; Jiang, M.; Huang, Y.; Li, J. Nanocrystalline Li-Al-Mn-Si Foil as Reversible Li Host: Electronic Percolation and Electrochemical Cycling Stability. *Nano Lett.* **2020**, *20*, 896−904.

(57) Hartmann, P.; Leichtweiss, T.; Busche, M. R.; Schneider, M.; Reich, M.; Sann, J.; Adelhelm, P.; Janek, J. Degradation of NASICON-Type Materials in Contact with Lithium Metal: Formation of Mixed Conducting Interphases (MCI) on Solid Electrolytes. *J. Phys. Chem. C* **2013**, *117*, 21064−21074.

**Supporting Information**

# Sacrificial Poly(propylene carbonate) Membrane for Dispersing Nanoparticles and Preparing Artificial Solid Electrolyte Interphase on Li Metal Anode

Qipeng Yu[a,b], Weicong Mai[a], Weijiang Xue[c], Guiyin Xu[c], Qi Liu[a,b], Kun Zeng[a], Yuanming Liu[a,b], Feiyu Kang[a,b], Baohua Li[a,*], Ju Li[c,*]

a. Shenzhen Key Laboratory on Power Battery Safety Research and Shenzhen Geim Graphene Center, Tsinghua Shenzhen International Graduate School, Shenzhen 518055, China.

b. School of Materials Science and Engineering, Tsinghua University, Beijing 100084, China.

c. Department of Nuclear Science and Engineering and Department of Materials Science and Engineering Massachusetts Institute of Technology, Cambridge, Massachusetts, 02139, United States.

*Corresponding authors.
E-mail: libh@mail.sz.tsinghua.edu.cn；
liju@mit.edu

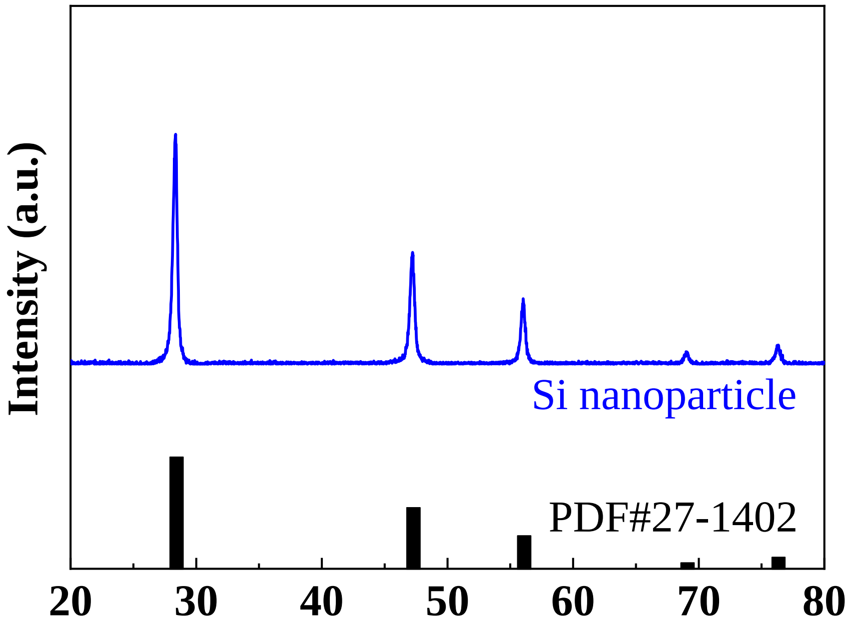

**Figure S1.** XRD pattern of Si nanoparticle (PDF#27-1402).

The diffraction peaks in Fig. S1 were characterized as Si (Fd-3m space group (JCPDS no. 27-1402)) with diffraction peaks at 28.4°, 47.3°, 56.1°, 69.1° and 76.4°. This result indicates that the applied Si nanoparticle is compose of pure Si without other impurities.[1]

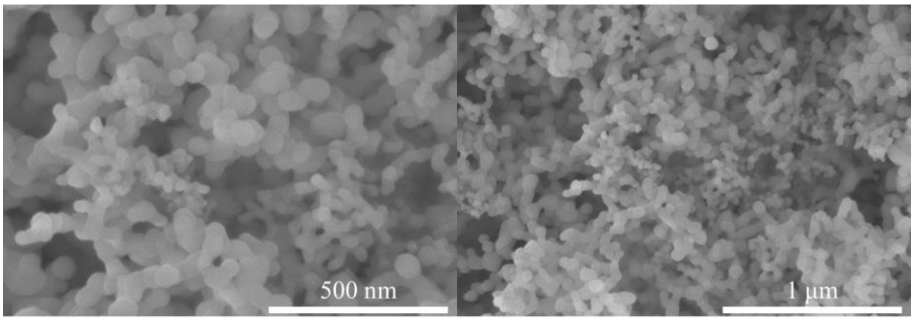

**Figure S2.** SEM images of Si nanoparticle.

The size of Si primary particle is mainly less than 100 nm, which can be regarded as nanoparticle.

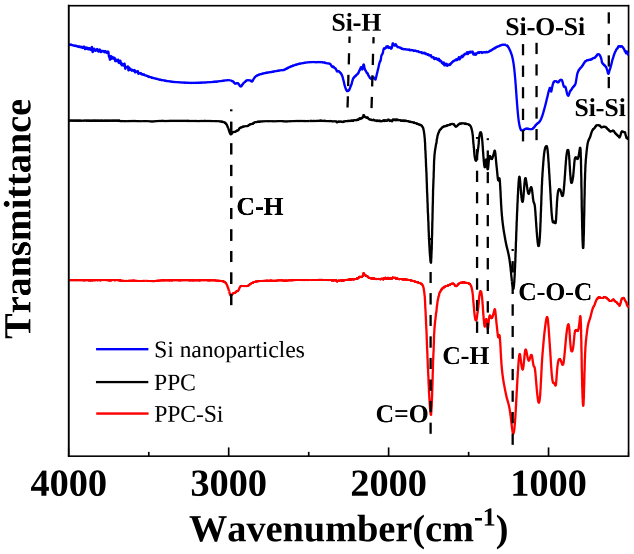

**Figure S3.** FT-IR spectroscopy of Si nanoparticle, PPC membrane and PPC-Si composite membrane.

The FT-IR of Si nanoparticle in Fig. S3 reveals the presence of various silicon crystal modes including a Si-O-Si mode at ~1110 cm$^{-1}$, SiH$_x$ stretching modes at ~2140, and 2090 cm$^{-1}$, Si-Si crystal mode at ~630 cm$^{-1}$.[2] For PPC membrane, we can see the typical characteristic absorption bonds of PPC, such as, the C=O stretching vibration located at 1742 cm$^{-1}$, the characteristic C-O-C bond at 1220 cm$^{-1}$.[3] The characteristic bonds of Si are not shown in PPC-Si may due to the relatively low amount of Si in PPC (only 2 % wt. ) and the overlap of characteristic bonds, like Si-O-Si bond.

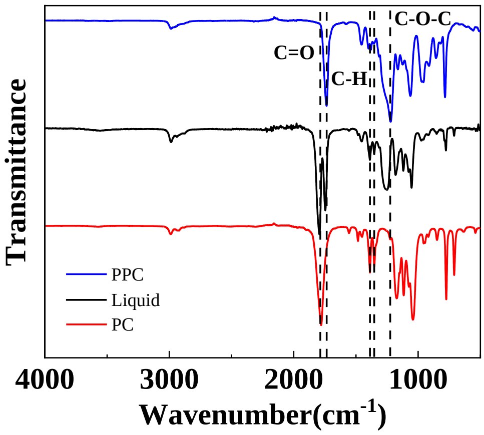

**Figure S4.** FT-IR spectroscopy of PPC membrane, liquid generated by PPC contacted with lithium metal and pure PC.

After contact with Li metal with heating and sufficient time, solid PPC membrane was changed into liquid. The liquid was collected and characterized by FT-IR. The characteristic C-O-C band at 1222 cm$^{-1}$ of pristine PPC shifted after changing into liquid. A strong vibrational band of C=O group located at ~1780 cm$^{-1}$ appeared, which was well corresponding to the pure PC, and the C=O stretching vibration of pristine PPC also appeared. The doublet band with two strong peaks at ~1387 cm$^{-1}$ and ~1353 cm−1 appeared in the obtained liquid ascribed to C-H wagging and symmetrical C-H bending modes, respectively, which was also the same as that of pure PC. The characteristic peaks of PC also confirmed that PPC would depolymerize to small segments (even PC) after contact with lithium metal with heating and sufficient time.

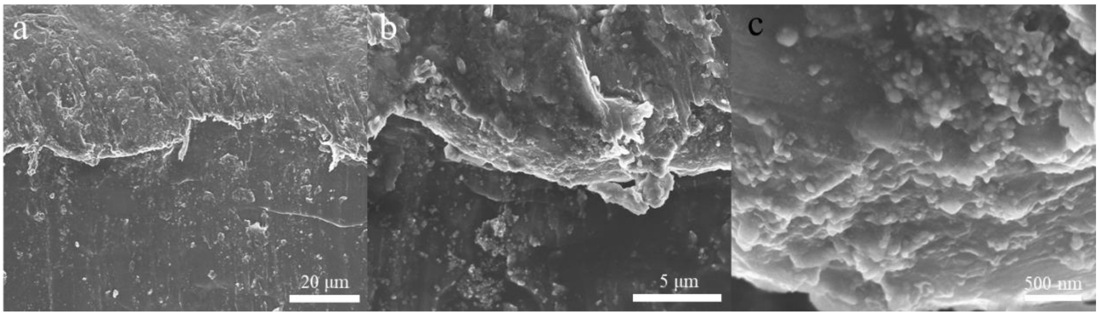

**Figure S5.** Cross-sectional SEM images of the PPC-Si-Li-H at different magnification.

A compact and uniform layer distinctly covered on top of the Li metal forming a protective layer as shown in Fig. S5a. Fig. S5b illustrated that the thickness of this layer was about 3 μm and Si nanoparticle could also be found in this layer in the high-magnification image in Fig. S5c. The volumetric ratio of this ASEI in the anode composite is ~ 0.6% and 5% for the 500 μm and 60 μm lithium foil, respectively.

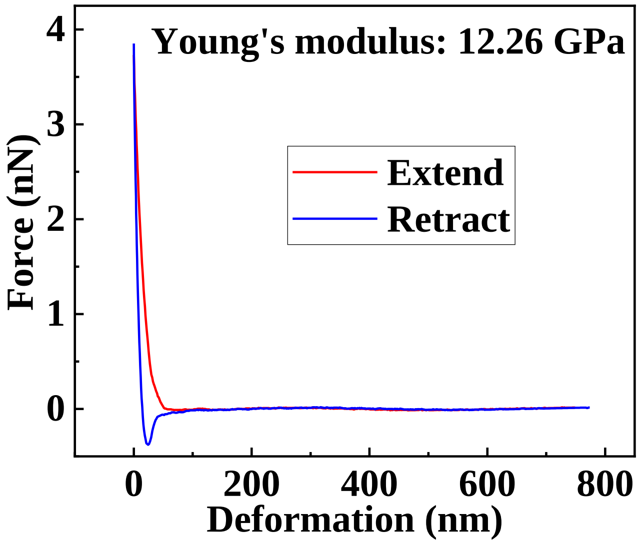

**Figure S6.** Force-displacement plots of PPC-Si-Li-H.

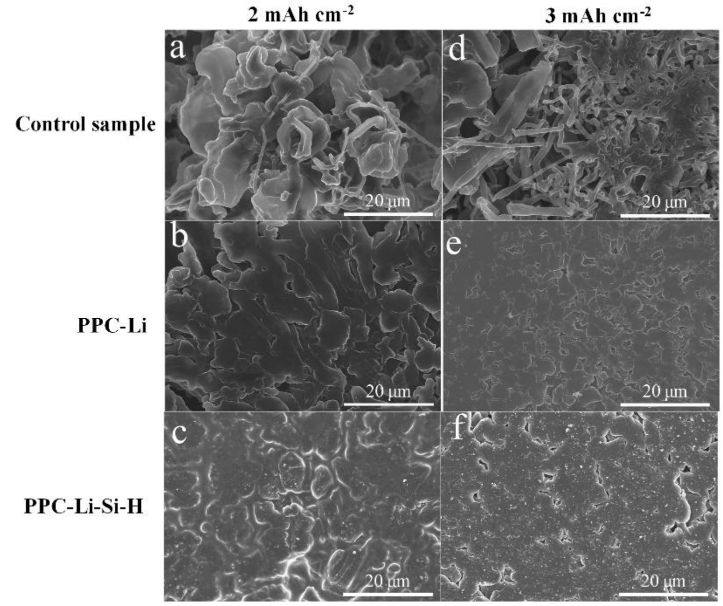

**Figure S7.** Surface morphology of LMA. SEM images of LMA at an areal deposition capacity of 2 mAh cm$^{-2}$ of (a) control sample, (b) PPC-Li and (c) PPC-Si-Li-H. SEM images of LMA at an areal deposition capacity of 3 mAh cm$^{-2}$ of (d) control sample, (e) PPC-Li and (f) PPC-Si-Li-H.

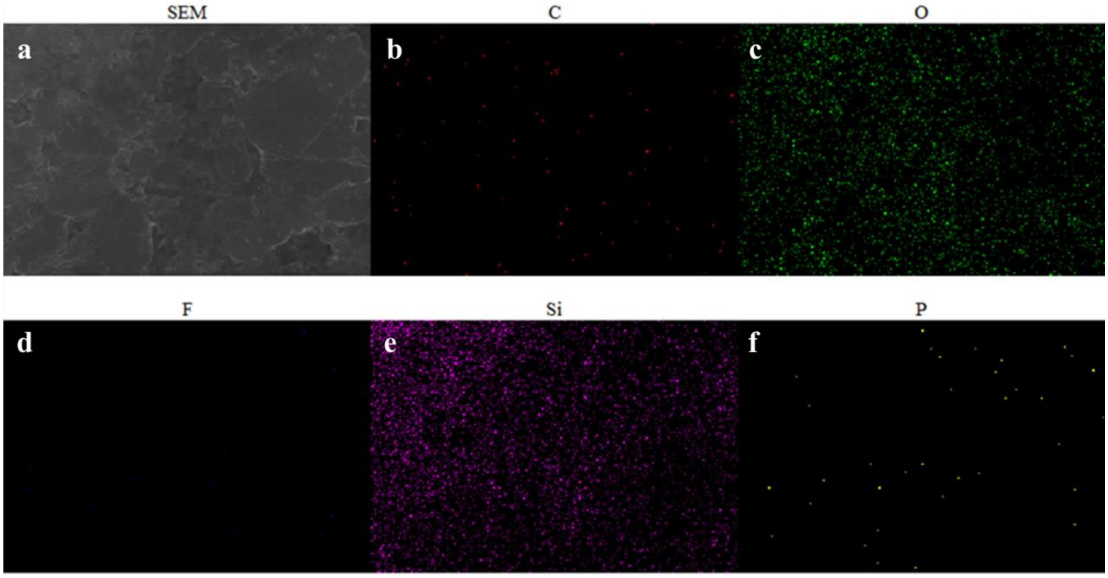

**Figure S8.** SEM image (a) of PPC-Si-Li-H after 100 cycles of 1 mAh cm$^{-2}$ deposition-dissolution process and corresponding EDS of Carbon (b), Oxygen (c), Fluorine (d), Silicon (e) and phosphorus (f) element.

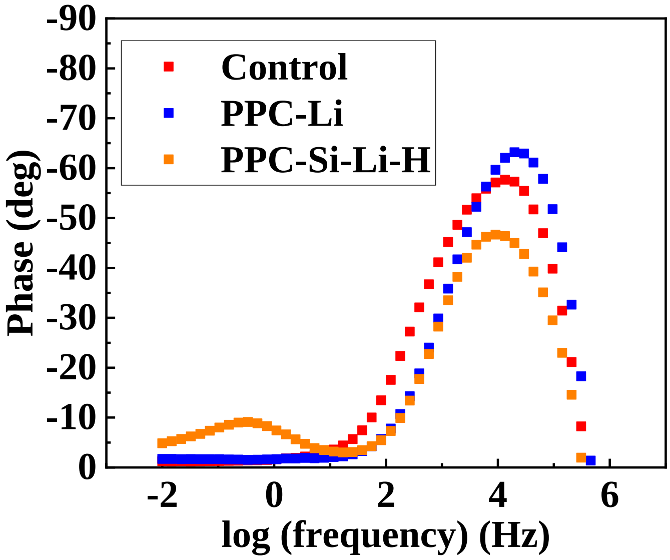

**Figure S9.** Bode impedance spectra of Control sample, PPC-Li and PPC-Si-Li-H after 1 hour intervals after cell assembly.

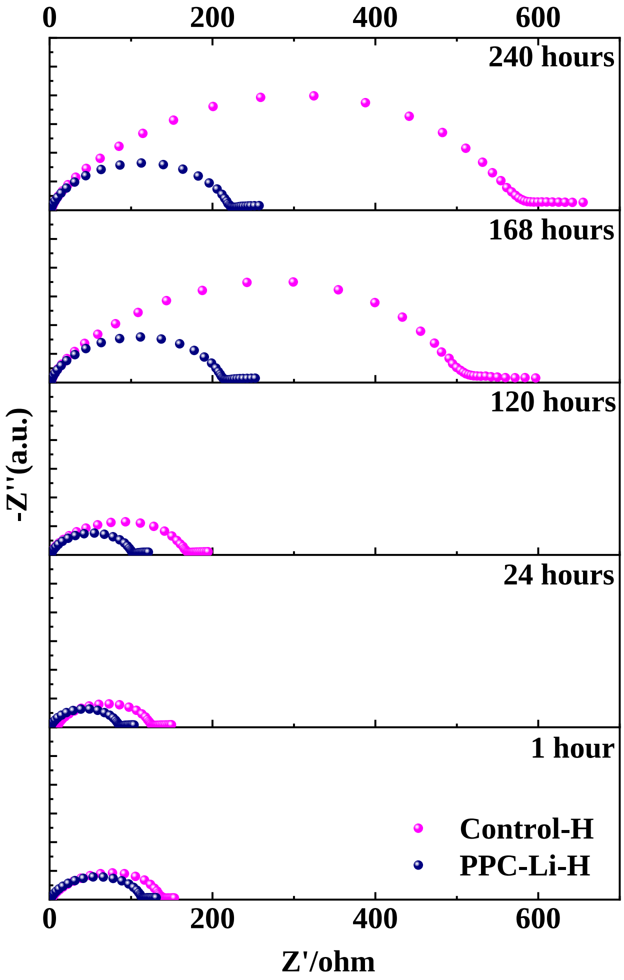

**Figure S10.** EIS plots of the symmetric cells after heating at 80 °C for 24 hours with different time intervals after cell assembly.

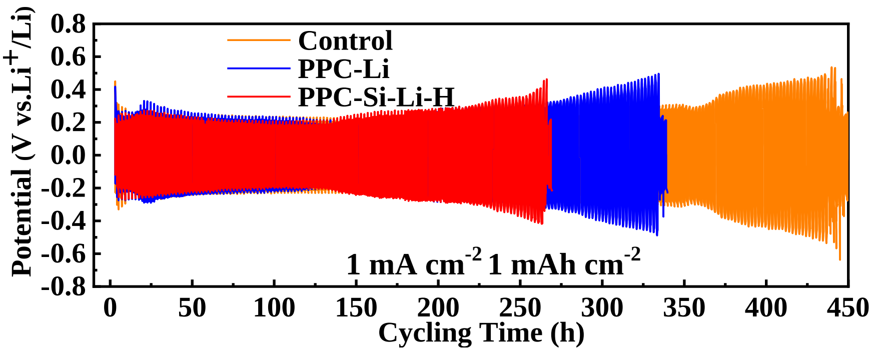

**Figure S11.** Lithium plating/stripping curves of symmetric cells at a current density of 1 mA cm$^{-2}$.

PPC-Li showed improved stability than the control samples, while PPC-Si-Li-80 exhibited the highest stability with over 350 hours of low polarization at 1 mA cm$^{-2}$. In comparison, the control samples only maintained stable for less than 150 hours at 1 mA cm$^{-2}$, indicating the remarkable improvement by such ASEI.

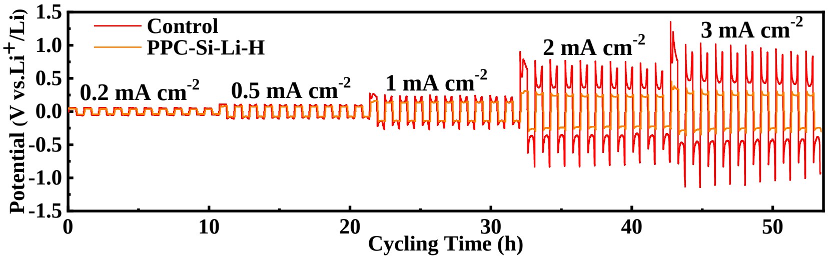

**Figure S12.** Lithium plating/stripping curves of symmetric cells at different current densities.

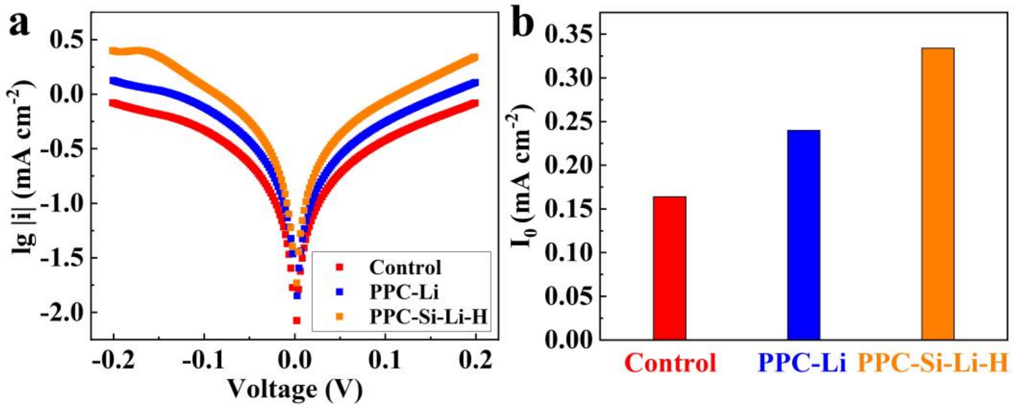

**Figure S13.** (a) Tafel plots obtained from cyclic voltammetry measurements at a scanning speed of 1 mV s$^{-1}$. (b) Comparison of exchange current densities ($I_0$) obtained from Tafel plots.

Additional proof that the charge-transfer kinetics are faster in the presence of ASEI fabricated by PPC sacrificial method can be seen from the exchange current densities ($I_0$). The $I_0$ values were calculated from the corresponding Tafel plots (Figure S13a). The Tafel plots were in turn obtained from cyclic voltammograms (CV) for symmetric Li cells. The results showed that the exchange current for Li deposition/stripping in PPC-Si-Li-H ($I_0$ = 0.334 mA cm$^{-2}$) and PPC-Li ($I_0$ = 0.240 mA cm$^{-2}$) are larger than what is achieved for the pristine Li ($I_0$ = 0.164 mA cm$^{-2}$). We suspect that the fast interfacial kinetics would facilitate low polarization during Li electrodeposition.

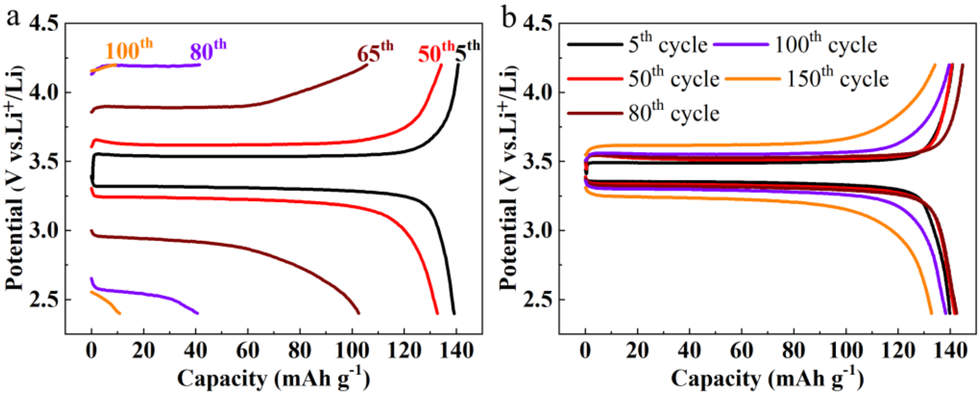

**Figure S14.** Charge-discharge curves in different cycles of LFP//Control (a) and LFP//PPC-Si-Li-H cell (b) from Fig. 5c.

For the control sample, polarization gently increased from the 5th to 50th cycle, then an outstanding increase of polarization was found in the 65th cycle. The polarization became too large for LFP cathode to deliver capacity in the 80th and 100th cycles, indicating the significant increase of resistance. Dendritic growth of lithium in the control sample would continuously consume electrolyte and form SEI, and the concomitant dead Li also increase the resistance. In sharp contrast, the polarization of PPC-Si-Li-H hardly increased from the 5th to 100th cycles, even in the 150th cycle, the polarization was still low. This results also demonstrated the benefits from the uniform deposition and suppress dendritic growth by such ASEI.

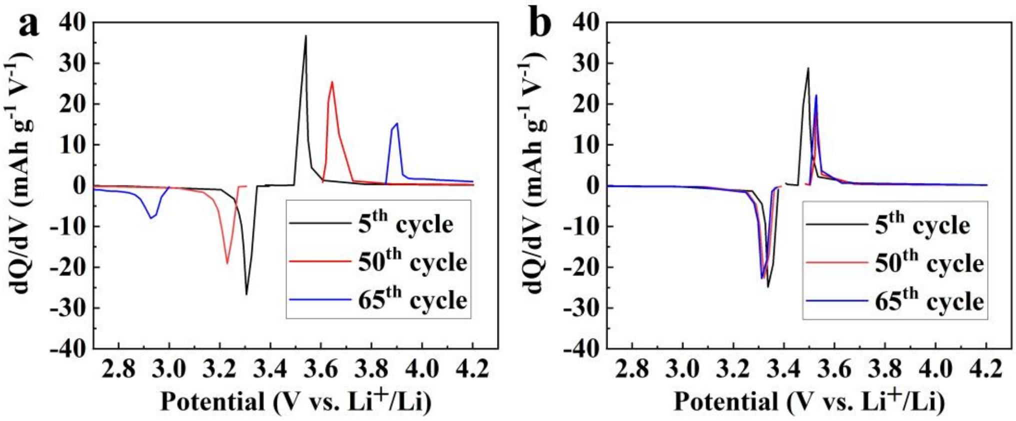

**Figure S15.** dQ/dV plots in different cycles of LFP//Control (a) and LFP//PPC-Si-Li-H cell (b).

The dQ/dV plots can provide more details of the reversibility of the electrochemical process. The corresponding potential of the peaks indicated the reaction potential. For the control sample, the oxidative and reductive potential was located at 3.54 V and 3.31 V, respectively, in the 5th cycle, indicating good reversibility. However, the oxidative potential in the 50th and 65th cycle shifted to 3.64 V and 3.90 V, respectively, while the reductive potential in the 50th and 65th cycle shifted to 3.23 V and 2.93 V, respectively. The oxidative potential shifted to higher and higher potential while the reductive potential shifted to lower and lower potential, indicating poorer reversibility. In sharp contrast, for PPC-Si-Li-H, the oxidative and reductive potential was located at 3.50 V and 3.34 V, respectively, in the 5th cycle, and shifted a little bit to 3.53 V and 3.32 V, respectively, in the 50th cycle. In addition, the peaks in the 65th cycle almost overlapped with that of the 50th cycle. All these results proved the enhanced stability by such ASEI.

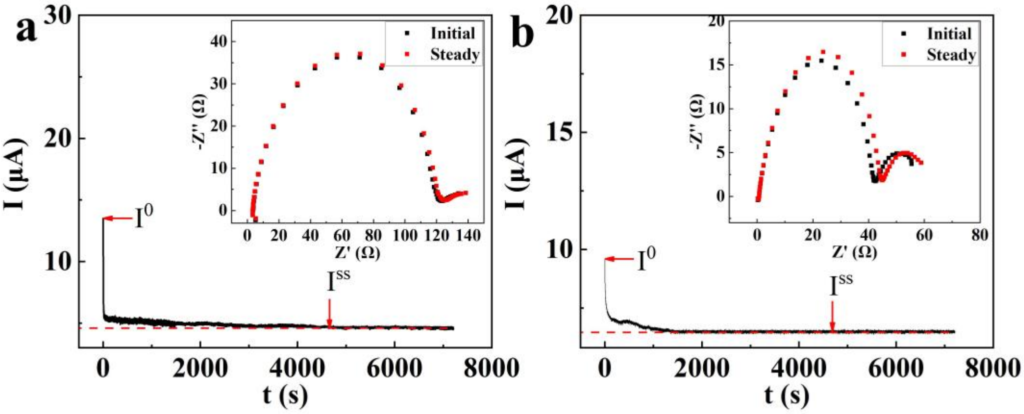

**Figure S16.** The chronoamperometry profile of control (a) and PPC-Si-Li-H symmetric cells under a polarization voltage of 10 mV, and the corresponding EISs before and after polarization (inset).

The transference number for the cation $t_+$ is given by:[4]

$$t_+ = \frac{I_{ss}(\triangle \mathrm{V} - I_0 R_0)}{I_0(\triangle \mathrm{V} - I_{ss} R_{ss})}$$

where $I_{ss}$ is the steady-state current, $I_0$ the initial current, △V the applied potential, $R_{ss}$ and $R_0$ the electrode resistances after and before the polarization, respectively. Therefore, the lithium transference number could be calculated as 0.35 and 0.64 for the control sample and PPC-Si-Li-H, respectively.

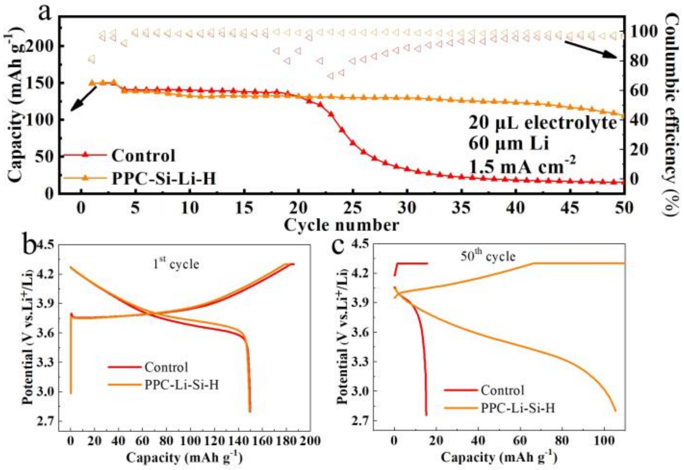

**Figure S17.** Cycling performance of NCM/Li cell with less electrolyte and anode (a), corresponding charge-discharge curves in the first cycle (b) and 50th cycle (c).

## Reference

(1) Tian, H.; Tan, X.; Xin, F.; Wang, C.; Han, W. Micro-sized nano-porous Si/C anodes for lithium ion batteries. *Nano Energy* **2015,** *11*, 490-499, DOI: 10.1016/j.nanoen.2014.11.031.

(2) Mawhinney, D. B.; Glass, J. A.; Yates, J. T. FTIR study of the oxidation of porous silicon. *The Journal of Physical Chemistry B* **1997,** *101* (7), 1202-1206.

(3) Wang, C.; Zhang, H.; Li, J.; Chai, J.; Dong, S.; Cui, G. The interfacial evolution between polycarbonate-based polymer electrolyte and Li-metal anode. *J. Power Sources* **2018,** *397*, 157-161, DOI: 10.1016/j.jpowsour.2018.07.008.

(4) Zugmann, S.; Fleischmann, M.; Amereller, M.; Gschwind, R. M.; Wiemhöfer, H. D.; Gores, H. J. Measurement of transference numbers for lithium ion electrolytes via four different methods, a comparative study. *Electrochim. Acta* **2011,** *56* (11), 3926-3933, DOI: 10.1016/j.electacta.2011.02.025.